Article:

Szewczyk, K.M., Panić, O., Iglesias, D.P. et al. (2026) HD 44892: the youngest (or oldest?) gas-harbouring debris disc around an intermediate-mass star. Monthly Notices of the Royal Astronomical Society, 545 (3). staf2150. ISSN: 0035-8711

https://doi.org/10.1093/mnras/staf2150

Monthly Notices of the ROYAL ASTRONOMICAL SOCIETY
MNRAS **545,** 1–13 (2026) https://doi.org/10.1093/mnras/staf2150
Advance Access publication 2025 December 03

HD 44892: the youngest (or oldest?) gas-harbouring debris disc around an intermediate-mass star

Karolina M. Szewczyk ,[1★] O. Panić ,[1] D. P. Iglesias ,[1] T. D. Pearce [2]
and J. M. Miley [3,4,5]

[1] *School of Physics & Astronomy, University of Leeds, Sir William Henry Bragg Building, Woodhouse Lane, Leeds LS2 9JT, UK*
[2] *Department of Physics, University of Warwick, Gibbet Hill Road, Coventry CV4 7AL, UK*
[3] *Departamento de Física, Universidad de Santiago de Chile, Av. Victor Jara 3659, Santiago 9170124, Chile*
[4] *Millennium Nucleus on Young Exoplanets and their Moons (YEMS), Chile*
[5] *Center for Interdisciplinary Research in Astrophysics Space Exploration (CIRAS), Universidad de Santiago de Chile, Satntiago 9170124, Chile*

Accepted 2025 November 25. Received 2025 November 25; in original form 2025 January 10

ABSTRACT

We present the first detections of gas around a 2.1 Myr old debris disc-bearing intermediate-mass star, HD 44892. Gas is detected both in ^{12}CO (2−1) emission through ALMA (Atacama Large Millimeter/submillimeter Array) Band 6 observations and in absorption in Ca II K and H, seen with high-resolution UVES (Ultraviolet and Visual Echelle Spectrograph) spectroscopy. ^{13}CO and C^{18}O (2−1) are not detected. The star exhibits a 12 µm fractional excess of $7.86^{+0.11}_{-2.27}$, placing it in the transition stage between protoplanetary and debris discs. Our detection of 1.3 mm emission yields the dust mass of $0.019 \pm 0.009\,M_{\oplus}$ assuming 115 K temperature. The ^{13}CO non-detection places an upper limit on CO gas mass of $\sim 10^{-2}\,M_{\oplus}$. The ^{12}CO detection yields a CO gas mass of $(7.86 \pm 2.05) \times 10^{-5}$ or $(1.62 \pm 0.17) \times 10^{-4}\,M_{\oplus}$ assuming a gas temperature of 20 or 50 K, respectively. These should be considered as lower limits since ^{12}CO emission may be optically thick. With UVES, we find variability in Ca II K and H lines, which can be interpreted by transiting circumstellar gas, ruling out interstellar absorption as their origin. Both the dust mass, which is within an order of magnitude of HD 141569, and the gas mass derived here indicate a late gas dispersal stage of the protoplanetary disc. Through our analysis, we deem the alternative age of 800 Myr unlikely.

Key words: exoplanets – planets and satellites: formation – protoplanetary discs – circumstellar matter – stars: pre-main-sequence – submillimetre: planetary systems.

1 INTRODUCTION

While the dust content of debris discs has been extensively studied, less is known about the presence of gas. Numerous papers have searched for and examined this gas presence (e.g. S. Marino et al. 2016; A. Moór et al. 2017; D. Iglesias et al. 2018; A. Moór et al. 2019; A. S. Hales et al. 2022; I. Rebollido et al. 2022; G. Cataldi et al. 2023); however, many questions remain unanswered. Perhaps the biggest question of all is: where does this gas come from? Two main scenarios have been proposed. This gas is either primordial, leftover from the parent protoplanetary disc (PPD), or secondary, produced alongside dust, through processes such as planetesimal collisions, volatile sublimation, and photodesorption (A. M. Hughes, G. Duchêne & B. C. Matthews 2018). Recent findings regarding the shielding effects in discs suggest that CO gas may accumulate in relatively high amounts from secondary means alone (Q. Kral et al. 2019). None the less, the primordial origin has not yet been disproved, especially as the effects of gas mixing complicate the case for the secondary gas scenario, making shielding less efficient (S. Marino et al. 2022), and models of R. Nakatani et al. (2021) suggest that, in case of A-type stars, the gas can survive as a protoplanetary remnant.

As of 2025 August, 45 debris discs containing gas have been discovered either through gas emission or absorption. Over 20 of them have been observed with ALMA (Atacama Large Millimeter/submillimeter Array) to search for CO and other gas emission, a full list of which can be found in Table A1. Interestingly, the majority of all gas detections in debris discs have been around A-type stars (see Fig. 1). For most of these systems, secondary origin models can readily explain the observed low CO gas masses. However, a few systems, such as 49 Cet (45 Myr, A. Moór et al. 2019; T. D. Pearce et al. 2022), HD 21997 (42 Myr, Á. Kóspál et al. 2013; A. Moór et al. 2013), HD 141569 (5 Myr, J. M. Miley et al. 2018), and HD 32297 (< 30 Myr, A. Moór et al. 2019), which are intermediate-mass stars (IMSs), exhibit significantly higher CO gas masses, which the current secondary models are not able to fully explain. In these cases, the origin of the gas is proposed to be primordial or a mixture of primordial and secondary (G. Cataldi et al. 2023). Secondary origin is most certain around older systems, such as the 440 Myr Fomalhaut (L. Matrà et al. 2017a) or the 1–2 Gyr η Crv (S. Marino et al. 2017), where primordial gas cannot survive over such long time-scales. β Pic, despite its younger age of ∼20 Myr,

★ E-mail: py19k2ms@leeds.ac.uk

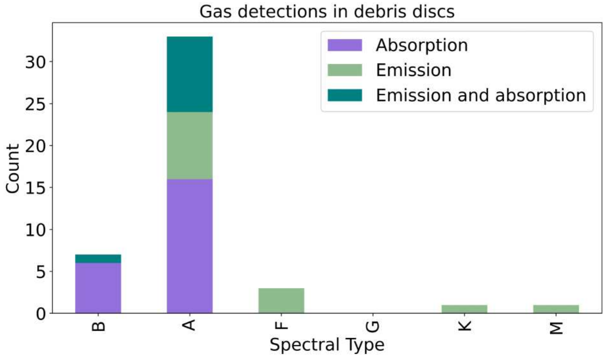

Figure 1. Histogram of all gas detections in debris discs through either emission or absorption, divided into bins of stellar type. For a full list of objects with gas emission, see Table A1. Objects with gas absorption used in this figure were adopted from D. Iglesias (2020, table 1.1), based on data from C. H. Chen & M. Jura (2003), A. M. Lagrange-Henri et al. (1990), H. A. Abt & K. I. Moyd (1973), B. Y. Welsh & S. Montgomery (2013), P. Koubsky et al. (1993), D. Iglesias et al. (2018), D. P. Iglesias et al. (2019), B. Y. Welsh et al. (1998), B. Y. Welsh & S. L. Montgomery (2015, 2018), and S. L. Montgomery & B. Y. Welsh (2012).

is another example of a system with secondary gas, in which gas produced in planetesimal collisions and the destruction of volatile bodies has been observed (W. R. F. Dent et al. 2014; L. Matrà et al. 2017b).

The primordial origin has been suggested for discs where the gas is present in substantial amounts – quantities that are not yet fully explainable by models of secondary origin – and where the parent star is very young (primordial gas is possible in systems < 50 Myr-old in models of R. Nakatani et al. 2021), hence the gas might not have yet been fully cleared from the system (G. V. Smirnov-Pinchukov et al. 2022). Such is the case for HD 141569 (J. M. Miley et al. 2018), a 5 Myr star harbouring a 'hybrid' disc, name used for gas-bearing discs with PPD levels of likely primordial gas, but debris-disc levels of secondary dust. These discs are similar to dusty debris discs but retain some primordial gas from the earlier evolutionary stage, hence are hybrid between PPD and debris discs (J. Péricaud et al. 2017). The dissipation of primordial gas is still ongoing in these systems, placing them just at the end of PPD dispersal. In the case of HD 141569, the dust is of secondary origin or mixed, with a relatively low dust mass and infrared (IR) excess for a PPD but high for a debris disc (Fig. 2), while the gas is suspected to be primordial and at a mass comparable to the least-massive PPDs. HD 141569 is thus the only known gas-harbouring debris disc found around a pre-main-sequence (pre-MS) IMS with a measured CO mass to date.

2 HD 44892

In this paper, we present ALMA observations of HD 44892 (also known as HIP 30414), an A9/F0IV type star (SIMBAD astronomical database - Set of Identifications, Measurements, and Bibliography for Astronomical Data, M. Wenger et al. 2000) located 191 ± 1 pc away (Gaia Collaboration 2016, 2023). HD 44892 has a temperature of 7500 ± 500K, a luminosity of $60.0 \pm 20.0\,L_{\odot}$, stellar mass of $2.87^{+0.67}_{-0.41}\,M_{\odot}$, and an age of $2.1^{+1.2}_{-1.0}$ Myr (D. P. Iglesias et al. 2023). The pre-MS star HD 44892 has undergone the transition from convective to radiative structure at ~1 Myr. G. A. Gontcharov (2006) have calculated the radial velocity of the star to be $20.9 \pm 0.6\,\mathrm{km\,s^{-1}}$, which is the value adopted in this study. A more recent estimate yields a value of $20.88 \pm 1.85\,\mathrm{km\,s^{-1}}$ (D. Iglesias, private communication), which is consistent with previous findings. There are no mentions in the literature suggesting HD 44892 is part of a binary or multiple star system; it is also a field star (J. Gagné et al. 2018).

D. Ishihara et al. (2017) identified it as a warm debris disc candidate based on its IR excess at 18 μm found through spectral energy distribution (SED) fitting, and it was first identified as a hybrid disc candidate in D. P. Iglesias et al. (2023). HD 44892 has a fractional IR excess at 12 μm of $7.86^{+0.11}_{-2.27}$ (D. P. Iglesias et al. 2023), placing it between debris disc ($3 < F_{12\mu m}/F_{\rm star}$) and PPD ($F_{12\mu m}/F_{\rm star} > 25$) (M. C. Wyatt et al. 2015; D. P. Iglesias et al. 2023), where also a number of gas-bearing debris discs have been found (Fig. 2, right).

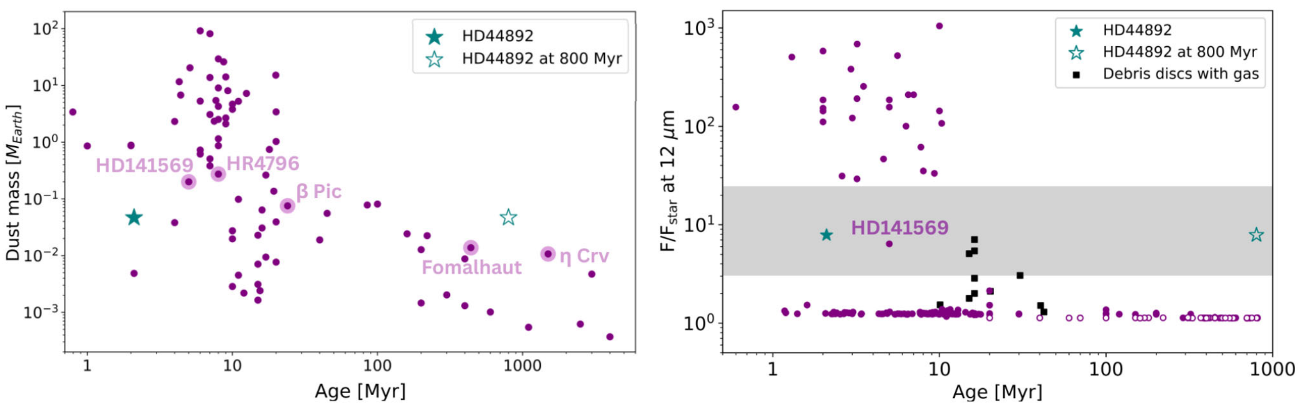

Figure 2. Left: evolution of dust mass in debris discs, originally presented in M. C. Wyatt et al. (2015). We have added more dust masses of debris discs, including those with gas discovered since. HD 44892 is marked with the two different possible ages: 2.1 and 800 Myr. At the older age, HD 44892 would have an unexpectedly high dust mass compared to other, older debris discs. Continuum fluxes used to create this plot were adopted from I. Sheret, W. R. F. Dent & M. C. Wyatt (2004); G. Sandell, D. A. Weintraub & M. Hamidouche (2011); O. Panić et al. (2013); J. Lieman-Sifry et al. (2016); A. Moór et al. (2017); T. D. Pearce et al. (2022); and L. M. Stapper et al. (2022), excluding systems with highly uncertain age estimates. The age of the HR 4796 was taken from J. H. Rhee et al. (2007). Dust temperature of 50 K is assumed for debris discs, and 25 K for PPDs, with a dust opacity assumed as $\kappa = 0.1 \times 2.3 \times (\frac{\nu}{230\times10^9})^{0.7}$ [cm^2 g^{-1}] (S. V. W. Beckwith et al. 1990), where ν is the frequency of observations [Hz]. Right: IR excess measured at 12 μm plotted as a function of age of the system, as originally presented in M. C. Wyatt et al. (2015, in purple, where open circles are upper limits), with additional data from A. Moór et al. (2017) of gas-bearing debris discs (in black). HD 44892 is again marked with the two possible ages, with the older age making it an outlier in the trend. The shaded region marks the stage between PPD and debris discs, where hybrid discs are expected to reside.

There is a disagreement in the literature regarding the stellar parameters of HD 44892, particularly about its age. Its location on the Hertzsprung–Russell (HR) diagram can be fit by either pre- or post-MS tracks. Past studies, such as J. Zorec & F. Royer (2012) and J. J. Bochanski et al. (2018), have classified it as a post-MS object (∼570–580 Myr with a mass of 2.50–2.60 $M_\odot$). D. P. Iglesias et al. (2023) present the fit to the pre-MS tracks yielding the 2.1 Myr and an alternative fit to the post-MS tracks with 800 Myr, with a mass of 2.29 $M_\odot$. They conclude that the possibility of the older age is less likely. In this paper, we adopt the pre-MS age of 2.1 Myr and present arguments against the alternative age of 800 Myr in later sections.

3 ALMA

3.1 ALMA observations and data reduction

HD 44892 was observed using the ALMA 12 m array on 2023 January 15 (PI: Panić, ID 2022.1.01686.S). Observations were taken across four spectral windows (SPWs) in Band 6, searching for both continuum and gas emission. The target was observed for a total of 34 min and 25 s using 46 operational antennas, with minimum and maximum baselines of 15.3 and 783.5 m, respectively. J0423−0120 was used as the flux calibrator and J0609−1542 as the phase calibrator.

Band 6 transitions of CO were observed, including the 2–1 transitions of ^{12}CO in an SPW of 1920 channels of width 244.141 kHz and a central frequency of 230 517 MHz, resulting in a resolution of 0.32 km s^{-1}. ^{13}CO and C^{18}O SPW has 1920 channels of width 976.562 kHz and a central frequency of 219 980 MHz, which gives a spectral resolution of 1.33 km s^{-1}. The remaining two SPWs, of central frequencies 216 980 and 232 979 MHz, were dedicated to continuum emission. Each of these windows contains 128 channels of width 15 625 kHz.

We processed all of the data using CASA 6.5.4–9 (J. P. McMullin et al. 2007) and CARTA 4.0.0 (A. Comrie et al. 2021). Continuum emission of HD 44892 was imaged using the task ‘tclean’ with Briggs weighting and a robust parameter set to 0.3, which we found to provide the highest signal-to-noise ratio and source emission over the range of −2 to 2 explored. Our target’s emission fits entirely in the region where primary beam is maximum, hence no primary beam correction was applied. No self-calibration was applied to the data as the source is too weak in continuum to provide reliable phase or amplitude solutions.

For line data, we used the CASA task ‘uvcontsub’ to subtract the continuum from the line emission data. Using the ‘plotms’ task (amplitude versus channel), we identified SPWs and frequencies at which line emission was potentially present. We imaged both SPWs using the ‘tclean’ task with Briggs weighting and a robust parameter set to 0.3, which produced the highest signal-to-noise ratio for the ^{12}CO detection. We did not detect any emission in the individual channels of the SPW containing ^{13}CO and C^{18}O.

3.2 ALMA results

3.2.1 Continuum

For continuum of HD 44892 our data reduction resulted in a synthesized beam size of 0.44 arcsec (84 au) × 0.38 arcsec (72 au) at a position angle (PA) of −70.7°. We detected continuum emission of 0.136 ± 0.016 mJy (∼9σ), shown in Fig. 3. The continuum flux was measured only from inside the 3σ contour. Using task ‘imfit’, which is part of the CASA package, we found that the continuum emission of HD 44892 is marginally resolved, as the fitted Gaussian component has an FWHM (full width at half maximum) of major axis of 0.58 arcsec ± 0.08 arcsec, 110 au, which extends beyond that of the beam (0.43 arcsec, 82 au, measured in the same direction). The drop in amplitude at longest UV distances (Fig. 4), confirms that the most extended emission from the source is being resolved.

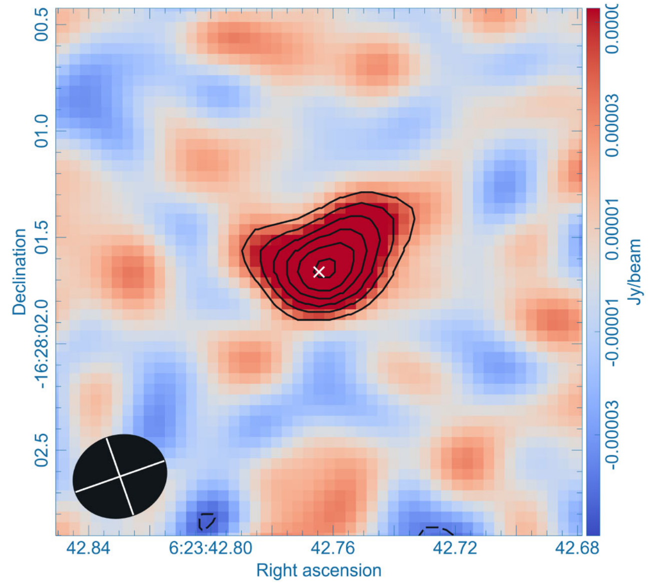

Figure 3. Continuum emission of HD 44892, marked in contours of (± 2, 3, 4, 5, 6, 7) × σ, where σ = 0.016 mJy beam^{-1}. Position of HD 44892 marked as a white cross.

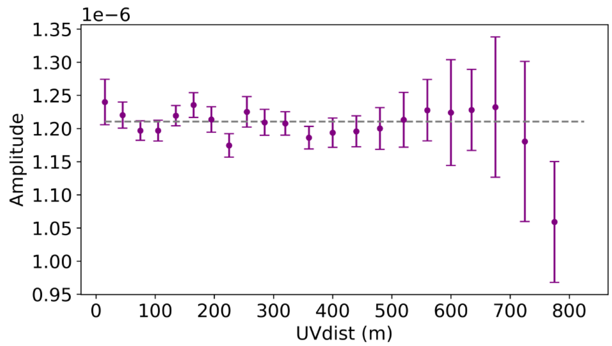

Figure 4. Amplitude versus UVdist plot of continuum of HD 44892. While the shorter UV-distance baselines can be fit with a straight line (dashed grey), hence are unresolved, the longest UV-baselines cannot, hence are not unresolved and deviate from a point-like source. The few points shown here correspond to the full continuum data set that has been averaged in time, channels, and binned by UVdist for clarity.

The continuum emission appears to be offset from the position of HD 44892 (see Fig. 3). To determine the underlying cause of this apparent offset, we calculated the astrometric accuracy of ALMA[1] using equation (1):

$$\sigma_{\rm pos} = \frac{\theta_{\rm FWHM}}{0.9 \times {\rm SNR}} \quad (1)$$

where $\theta_{\rm FWHM}$ is the FWHM of the synthesized beam, and SNR is the signal-to-noise ratio of the peak target flux. For our data, we

[1] https://help.almascience.org/kb/articles/what-is-the-absolute-astrometric-accuracy-of-alma

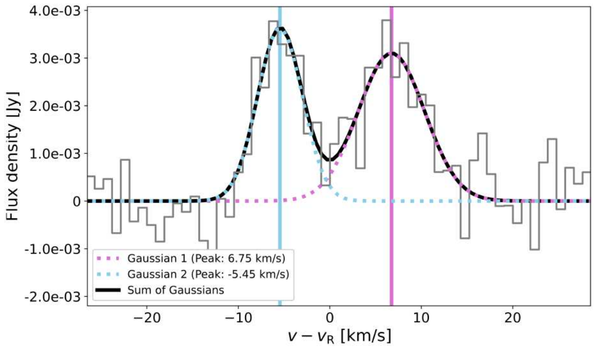

Figure 5. Radial velocity spectrum of ^{12}CO emission with peak positions marked. The *x*-axis has been corrected for the star's radial velocity in the LSR frame of ∼1.5 km s^{-1}.

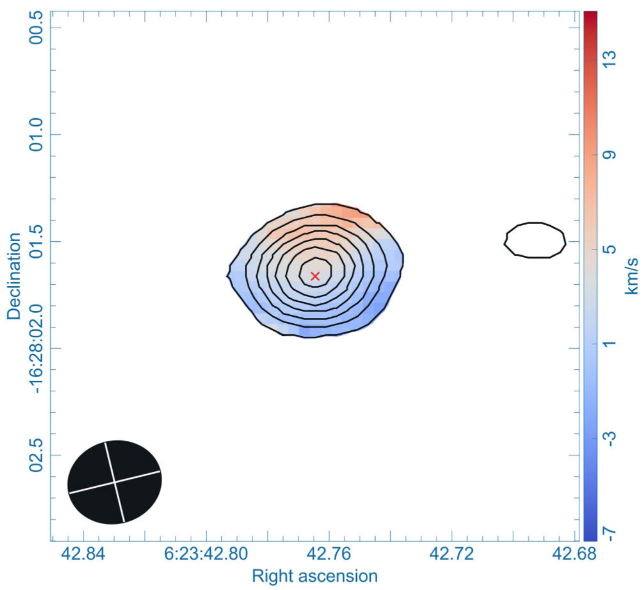

Figure 6. Integrated ^{12}CO 2–1 line intensity of HD 44892 with contours of (2, 3, 4, 5, 6, 7, 8) × σ, where σ = 11.01 mJy beam^{-1} km s^{-1}. Position of HD 44892 marked as a cross. Contours are integrated intensity (moment 0), while colour scale is from intensity-weighted coordinate (moment 1), only shown for > 2σ emission from the source.

found σ_{pos} = 45 mas. The apparent offset of the continuum emission from the stellar position is 34 mas, which is less than the calculated σ_{pos}, suggesting that it is most likely due to the limited astrometric accuracy rather than physical displacement.

3.2.2 Gas

For ^{12}CO emission, the resulting synthesized beam size is 0.46 arcsec (88 au) × 0.40 arcsec (76 au), at a PA of −80.6°. Fig. 5 shows the spectrum of the detected gas emission, which has the typical double-peaked profile associated with gas rotating in a Keplerian disc. Fitting a double-peaked Gaussian curve to this spectrum reveals a mid-point at v = ∼0 km s^{-1}. The first peak is at −5.45 km s^{-1} and the second at 6.75 km s^{-1}. This *x*-axis of this plot has been corrected for the star's radial velocity in the LSR (local standard of rest) frame of ∼1.5 km s^{-1}.

From moment 0 (Fig. 6, integrated intensity made using the CASA task 'immoments' within range −8.49 to 15.33 km s^{-1}) we found an integrated line flux of 96.92 ±16.22 mJy km s^{-1} (∼6.0 σ). Therefore, we decided to re-image the data, this time binning three channels together during tclean (nchan = 3). This reduced the noise in our image and made the emission more prominent. The moment 0 map was made using the same velocity range as in the non-binned case, resulting in a slightly lower noise of 14.10 mJy km s^{-1}, and the integrated line flux of 93.06 mJy km s^{-1}, improving the signal-to-noise ratio (6.6σ).

We then also used the Keplerian Mask tool,[2] which produces a rotating mask based on the system's parameters that a Keplerian disc should follow. To search the parameter space to be used in the tool, we are guided by the aspect ratio of the deconvolved disc size. We used the 'imfit' task and obtained the deconvolved Gaussian parameters: 0.34 arcsec ± 0.10 arcsec for the major axis and 0.19 arcsec ± 0.08 arcsec for the minor axis (PA of 76.2 ± 63.4°). This suggests an inclination of 56.1 ± 19.9°. We therefore varied the inclination from 36° to 76° in the Keplerian Mask tool. The stellar mass range was adopted from D. P. Iglesias et al. (2023) as $2.87^{+0.67}_{-0.41}$M$_\odot$ and Keplerian rotation computed accordingly in the tool. Using these values as initial constraints, we explored combinations of the parameters (within their uncertainty ranges) to best match the ^{12}CO emission of HD 44892. The parameters that resulted in the best fit were an inclination of 40°, PA of 17.2°, stellar mass of 3.27 M$_\odot$, and an outer radius of 0.4 arcsec (76 au). The ^{12}CO emission follows this rotation, indicating that the emission lines up with theoretical positions and confirming it is from a disc rotating around the parent star (Fig. 7). Using the Keplerian Mask during cleaning has improved the signal-to-noise ratio once more, in moment 0 this resulted in an integrated line flux (F_{21}) of 95.47 ± 13.49 mJy km s^{-1} (7.1σ, Fig. 6). Here, we used channels where gas emission was most prominent, corresponding to the frequency range of 230.5262 GHz (15.33 km s^{-1}) to 230.5445 GHz (-8.49 km s^{-1}).

Knowing the channels (velocities) at which ^{12}CO emission is present, we created a moment 0 map for the SPW containing ^{13}CO and C^{18}O. The emission from these isotopes would allow for a more precise CO gas mass calculation, as they are likely optically thin, ensuring the ^{12}CO emission traces molecular density, rather than being convoluted with temperature effects. Since no emission was visible in the individual channels of this SPW, we used the same velocity range as for ^{12}CO. However, this has resulted in a non-detection of both ^{13}CO and C^{18}O.

Fig. 6 shows the full extent of ^{12}CO gas emission (contour levels) overlaid on the velocity distribution of the disc. The visible velocity gradient, from red- to blueshifted, indicates gas rotation. This, along with the disc being located around the star's position, confirms the gas is rotating around the star and the emission is not from a different source. The gas emission appears compact and follows the beam shape, with the highest intensity near the centre, as expected for a spatially unresolved source.

4 UVES

4.1 UVES observations and data reduction

We obtained high-resolution observations of HD 44892 using UVES (Ultraviolet and Visual Echelle Spectrograph; H. Dekker et al. 2000) at the VLT (Very Large Telescope), on 2023 September 13 and 27 (PI: Iglesias, ID 112.262P.001). VLT is part of the European

[2]https://github.com/richteague/keplerian_mask

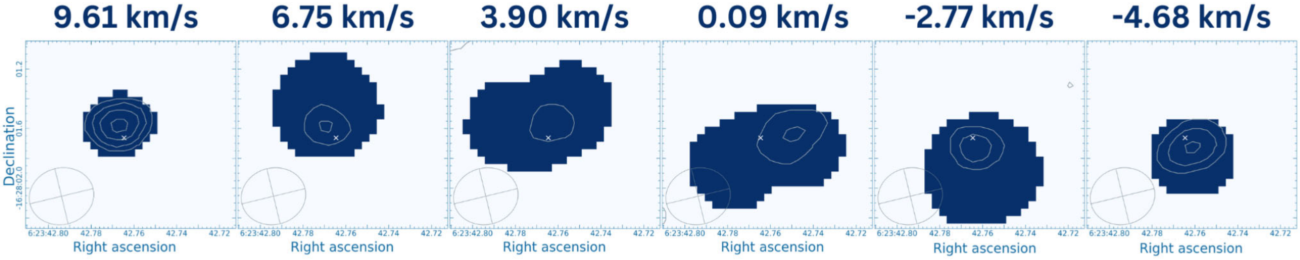

Figure 7. Contours of ^{12}CO emission of HD 44892 overlaid on top of the created Keplerian Mask. The gas emission rotates with the theoretical Keplerian motion around the host star. Channel contours start at 3σ ($\sigma = 1.60$ mJy beam^{-1}) with the exception of middle two panels which start at $2\,\sigma$.

Southern Observatory and is located in Cerro Paranal in Chile. Data were taken in both blue and red arms, centred at 390 and 580 nm, respectively. We used the 0.5 arcsec for these observations to achieve high resolution (R∼74 000 for the red arm and R∼65 000 for the blue arm). HD 44892 was observed each time for 1 min 48 s. Data of one of the comparison stars used, HIP 28877, is part of the same observing programme. The observations were reduced using the UVES ESOREFLEX pipeline (P. Ballester et al. 2000; W. Freudling et al. 2013) version 6.4.1.

Additional spectra from the ESO archive[3] were obtained for two other comparison stars (HD 43544 and HD 46035), using high-resolution spectrographs HARPS (High Accuracy Radial velocity Planet Searcher, M. Mayor et al. 2003) and FEROS (Fiber-fed Extended Range Optical Spectrograph, A. Kaufer et al. 1999) at the La Silla Observatory. These were science-ready products from the ESO archive and reduced with each instrument standard pipeline. We used MOLECFIT (W. Kausch et al. 2015; A. Smette et al. 2015) to correct for telluric contamination as the region around the Na I doublet is highly affected by the Earth's atmosphere. Barycentric radial velocity corrections were also applied to the spectra.

4.2 UVES results

Using data from the UVES spectrograph, we also searched for gas absorption towards HD 44892, particularly in the Ca II K and H, and Na I D1 and D2 lines. By fitting Kurucz model spectra to the stellar spectrum of our target, we identified a narrow absorption feature, located at 22.5 km s^{-1} (36σ, Fig. 8). Although this feature does not correlate with the radial velocity of any known gas clouds in the line of sight and falls within the stellar radial velocity range of 20.88 ± 1.85 km s^{-1}, it is matched well by several of the nearby comparison stars. Interstellar origin of this feature is further supported by its strength in both of the sodium lines, which are a strong indication of interstellar medium (ISM) gas presence. The detailed description of methods used and analysis of the absorption features of this and other objects will be published in Szewczyk et al. (in preparation).

There is, however, some variability in the residual flux present in both Ca II K and H lines (Fig. 8), which is not present in the sodium lines. This variability does not match with any of the clouds in the line of sight nor the nearby comparison stars. While not at the radial velocity of the parent star, this variability in the residual absorption might be caused by secondary gas released from volatile bodies like in case of β Pic (W. R. F. Dent et al. 2014) or a gas wind-disc, like the one found around NO Lup (J. B. Lovell et al. 2021b), although this cannot be confirmed with the data we currently have. Thus, it is possible we have detected variable, circumstellar gas around HD 44892.

Following the methods described in J. R. Fairlamb et al. (2017), we calculated the mass accretion rate of HD 44892 from the Hα spectrum. We found accretion rates of $\log \dot{M}_{\rm acc} = -7.64^{+0.11}_{-0.07}$and $-7.69^{+0.11}_{-0.07}$ M$_\odot$ yr^{-1} for the two observed epochs, which are consistent with those of other Herbig Ae/Be stars (C. Wichittanakom et al. 2020). This further suggests that HD 44892 is a pre-MS star, with an estimated age of 2.1 Myr, as accretion is characteristic of young stellar objects. Variability is also observed in the Hα line (Szewczyk et al., in preparation), similar to that seen in the Ca II K and H lines. Hence, the derived accretion rate may correspond to a temporary phase of high accretion and should therefore be regarded as an approximate estimate.

5 ANALYSIS AND DISCUSSION

5.1 ALMA

5.1.1 Continuum

The continuum emission we have detected around HD 44892 is only marginally resolved along the major axis. Because of this, we are unable to estimate the orbital distance to the debris disc using our current data, and hence cannot determine the dust temperature, on which dust mass depends. To provide a more reliable estimate of the dust mass, we have utilized the 'simalma' task, which is part of CASA package. We first created models, each containing a circular dust ring at various disc inclinations, located at a range of orbital distances from the star (with disc radii extending to 20–100 au along the major axis), which we then input into 'simalma'. Because the continuum emission is only marginally resolved, we did not consider the ring width as a free parameter and fixed it to 1 pixel (0.2 au), small enough to not influence the fit. The aim of our approach was to determine the dust ring size that would best mimic our observations – effectively, the maximum radius at which the dust can be placed without the belt becoming resolved. The simulations were carried out using the exact same observational setup as our real continuum observations – including observing time, precipitable water vapour (pwv), frequency, antenna setup, and other parameters – in order to accurately replicate the noise, resolution, and observed flux.

We used the CASA task 'imfit' to compare the simulated images to the actual data, and found that a ring located approximately 40–45 au from the star best reproduced the observed emission. Since the minor axis is not resolved, we cannot give an estimate to its size. Based on this distance, assuming the dust particles behave as blackbodies, we

[3]http://archive.eso.org

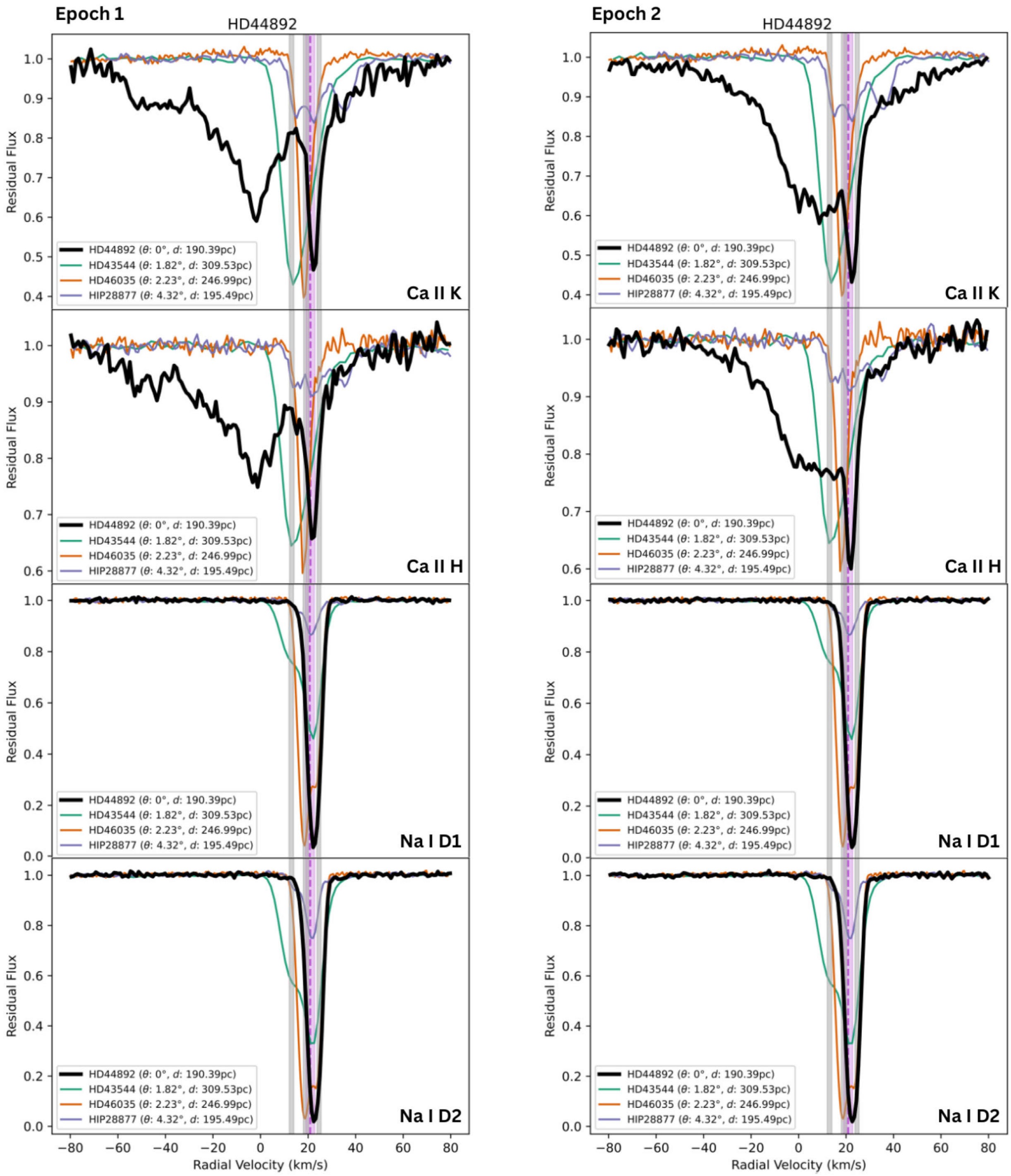

Figure 8. Narrow absorption features found in the spectra of HD 44892 overlaid with features found in the spectra of nearby stars, with their distances and separations from HD 44892 marked. Each row represents a different absorption line: Ca II K and H, and Na I D1 and D2. The two columns show observations from two different epochs. Shaded regions correspond to the radial velocities of known clouds in the line of sight, while the vertical dashed line marks the radial velocity of HD 44892, $20.88 \pm 1.85\,\mathrm{km\,s^{-1}}$, and its surrounding region represents the associated uncertainty. Variability between the two epochs is observed in the calcium (K and H) lines, but is absent in the sodium (D1 and D2) lines, spawning a radial velocity range of -70 to $15\,\mathrm{km\,s^{-1}}$. This variability may be caused by transiting, circumstellar gas. The pronounced narrow absorption feature at $22.5\,\mathrm{km\,s^{-1}}$ is most likely caused by interstellar gas, given its strength in both sodium lines and the close match with nearby stars' features in calcium lines.

estimated the dust temperature using equation (2):

$$R = \sqrt{\frac{\mathrm{L}_{\odot}}{16\pi\sigma T^4}} \tag{2}$$

where R is the distance from the parent star to the debris belt, $\mathrm{L}_{\odot}$ is the stellar luminosity, σ is the Stefan–Boltzmann constant, and T is the dust belt temperature. A debris belt distance of 40–45 au corresponds to a dust temperature of ∼115 K.

We calculated the minimum dust mass of HD 44892 assuming optically thin, thermal emission, with equation (3):

$$M_{\rm dust} = \frac{F_\nu \times D^2}{B_\nu(T) \times \kappa_\nu} \quad (3)$$

where F_ν is the source emission, D is the distance to the source, $B_\nu(T)$ is the *Planck* function (dependent on dust temperature, T), and κ_ν is the dust opacity, which is very uncertain. Here, we assume $\kappa = 0.1 \times 2.3 \times (\frac{\nu}{230\times10^9})^{0.7}$ [cm^2 g^{-1}] (S. V. W. Beckwith et al. 1990), where ν is the frequency of observations [Hz]. This results in a minimum dust mass at the dust temperature of 115 K of $0.019 \pm 0.009\,M_\oplus$. This mass is highly dependent on the dust temperature, which is uncertain given the emission is only marginally resolved along the major axis. For comparison, a lower dust temperature of 50 K would yield a higher dust mass estimate of $0.05 \pm 0.03\,M_\oplus$.

Based on the expected lifetime of the observed dust, we can estimate whether it is primordial (left over from system formation) or secondary (released in planetesimal collisions). In the absence of gas, the lifetime of millimetre dust would be dominated by grain–grain collisions. The longest time-scale at which this amount of millimetre dust can be destroyed, assuming collisions with dust of the same size, is if we distribute it in the entire region up to 40–45 au. In this scenario, following T. D. Pearce et al. (2021, equation 8, based on M. C. Wyatt & W. R. F. Dent 2002) we obtain the dust lifetime of order 10^{-2} Myr, which is much smaller than the estimated age of HD 44892. Whilst the derived lifetime could be extended in the presence of gas, which can damp grains and reduce their impact velocities, very significant damping would be required to extend the lifetime up the the 2 Myr star age. Hence the estimated lifetime, combined with the relatively low dust mass compared to PPDs (Fig. 2), leads us to believe that at least some of the dust is secondary in nature. This is typical for hybrid discs, which are thought to comprise primordial gas and second-generation dust (e.g. Á. Kóspál et al. 2013; A. Moór et al. 2013).

5.1.2 Gas

To calculate the CO gas mass in this disc we follow methods described in J. M. Miley et al. (2019) and L. Matrà et al. (2015). Since our detection is in ^{12}CO (2−1) only, we use equation (4) to calculate the minimum CO gas mass, assuming local thermodynamic equilibrium:

$$M_{\rm CO} = \frac{4\pi m d^2}{h\nu_{21} A_{21}} \frac{F_{21}}{x_2} \quad (4)$$

where F_{21} is the integrated flux of gas emission, d is the distance to the star, m is the mass of the emitting molecule (^{12}CO), ν_{21} is the rest frequency of the transition, h is *Planck*'s constant, A_{21} is the appropriate Einstein coefficient, and x_2 is the fraction of the population found in the upper level of the transition (in this case '2'), estimated using a Boltzmann distribution. Since the gas emission is spatially unresolved, we cannot estimate its temperature. Using the flux measured for ^{12}CO emission, for 20 K gas we obtain a minimum CO gas mass of $(7.86 \pm 2.05) \times 10^{-5}$ or $(1.62 \pm 0.17) \times 10^{-4}\,M_\oplus$ assuming warmer gas at 50 K.

Given the young age of HD 44892 and its transitional stage from a PPD to a debris disc, the primordial origin of gas cannot be ruled out (R. Nakatani et al. 2021). Primordial gas is leftover from the protoplanetary stage, where it is dominated by the ISM-like abundances of molecular hydrogen (H_2), with carbon monoxide (CO) along other gases contributing to the total gas mass. Assuming the disc is hybrid, we use the ISM ratio of ^{12}CO/H_2 = 10^{-4} to estimate the total gas mass in this disc, under the assumption of a substantial hydrogen presence in the disc. If the gas is indeed primordial, we estimate the H_2 mass, and hence total disc gas mass, to be $0.06 \pm 0.02\,M_\oplus$ for 20 K gas and $0.12 \pm 0.01\,M_\oplus$ for 50 K gas. These estimates are based on the lower limit of CO gas mass (estimated from ^{12}CO emission), hence the total gas mass in this disc may be higher.

Table 1. Upper limits to CO and total gas mass derived from ^{13}CO and C^{18}O non-detections, and lower limits from ^{12}CO emission.

In units of $M_\oplus$:	^{13}CO	C^{18}O	^{12}CO
$M_{\rm CO}$ (20K)	$<7.09 \times 10^{-3}$	$<5.27 \times 10^{-2}$	$(7.86 \pm 2.05) \times 10^{-5}$
$M_{\rm CO}$ (50K)	$<1.47 \times 10^{-2}$	$<1.10 \times 10^{-1}$	$(1.62 \pm 0.17) \times 10^{-4}$
M_{H_2} (20K)	<5.06	<37.67	0.06 ± 0.02
M_{H_2} (50K)	<10.51	<78.30	0.12 ± 0.01

From the moment 0 map made for the two non-detections, ^{13}CO and C^{18}O, we derived upper limits to the CO gas mass. By overlaying the 3σ contours of ^{12}CO emission on this map, we derived the RMS within this region to be 30.28 mJy km s^{-1}, with $3\sigma = 90.84$ mJy km s^{-1}, which we use as ^{13}CO and C^{18}O flux for the purpose of gas mass calculations, since the data set is common between them. We adopt the ISM-like relative ratios of CO/^{13}CO and CO/C^{18}O as 77 and 550, respectively (T. L. Wilson & R. Rood 1994). Using equation (4) with adjusted values for m and x_2, we obtained the upper limits to the CO gas mass as presented in Table 1. However, since in debris discs ^{13}CO is typically more abundant than C^{18}O (see e.g. J. M. Miley et al. 2018), the upper limit on the CO gas mass derived from ^{13}CO is more stringent. The total CO gas mass in the debris disc of HD 44892 should hence be contained between the lower limits from the ^{12}CO emission and upper limits from ^{13}CO non-detection.

5.1.3 Gas and dust emission morphology

Examining the structure of both the continuum and ^{12}CO emission (Fig. 9), we can see that the dust emission clearly has a different morphology than the ^{12}CO emission. This direct comparison in their morphology is possible because of the similar signal-to-noise ratio of both dust and ^{12}CO emission. The ^{12}CO integrated emission is not spatially resolved, therefore it follows the beam distribution. As mentioned in Section 3.2.1, the continuum emission is marginally resolved, which can be further seen in Fig. 4. Here, the longest UV-distance baselines, at ∼800 m, deviate from a flat profile, which indicates the continuum emission is not unresolved, since a point-like source would have a constant amplitude across all baselines. The extended continuum emission is only marginally resolved with an apparent asymmetry at a level of 4.5σ, which may or may not indicate asymmetry in the dust disc. The larger extent of continuum emission with respect to CO emission is atypical in PPDs, and more common in debris discs (e.g. A. Moór et al. 2019; E. Di Folco et al. 2020; S.-i. Inutsuka et al. 2023). Higher resolution observations are necessary to ascertain the distribution of dust and CO gas in the HD 44892 system.

5.2 SED

Fig. 10 shows the SED of the HD 44892 debris disc, assuming optically thin dust. The excess emission is best modelled with a single-temperature belt structure, fitted using a blackbody model. Due to the uncertainties in the temperature of the parent star

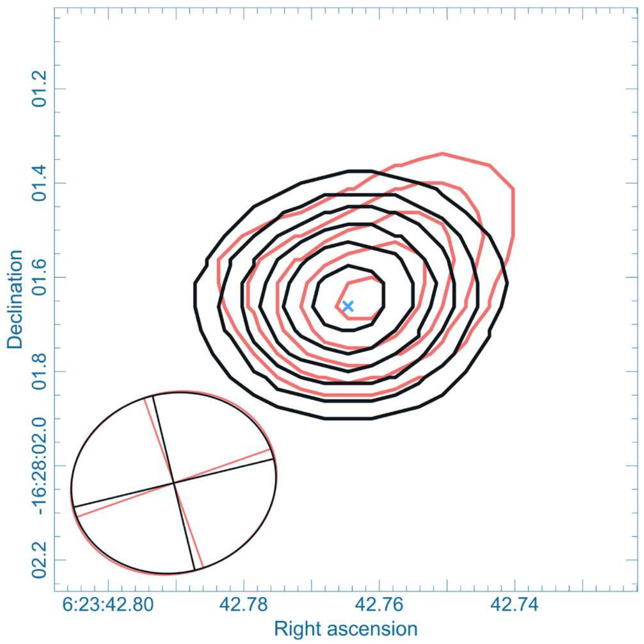

Figure 9. Overlaid contours of continuum (red) and CO emission (black) of HD 44892. CO emission marked in contours of (3, 4, 5, 6, 7, 8) × σ, where $\sigma = 11.01$ mJy beam^{-1} km s^{-1}, while continuum is (3, 4, 5, 6, 7) × σ, with $\sigma = 0.016$ mJy beam^{-1}. Position of HD 44892 marked as a cross.

$T_{\rm eff} = 7500 \pm 500$ K, we present the SED fit to the stellar temperature of 7500 K along with the alternative minimum and maximum values of 7000 and 8000 K. The fit to the excess is highly dependent on the assumed stellar temperature, changing the resultant dust-belt temperatures. The best-fitting SED (left plot of Fig. 10, 7000 K) suggests that the debris disc is composed of a warm belt at 739 K, based on which we estimate the location of this component belt using equation (2).

We estimate the distance of the 739 K dust belt to be 1.1 au from the parent star. The two higher temperature fits produce additional excess points that cannot be fitted with the existing blackbody component and would hence require an additional, even hotter belt fit. However, at such high temperatures, around A-type stars, it would be physically impossible for the dust to survive, suggesting the stellar fit might not be accurate. Carbon grains ~0.1 au away from A-type stars sublimate at ~2000 K (e.g. J. Lebreton et al. 2013; T. D. Pearce, A. V. Krivov & M. Booth 2020). Silicates sublimate at comparatively cooler temperatures of ~1200 K (e.g. É. Sezestre, J. C. Augereau & P. Thébault 2019). In addition to the SED data shown in Fig. 10, there exists a 100 μm upper limit listed in the *IRAS* catalogue, which we did not include in the SED fit, as it is very large and does not represent a meaningful constraint.

5.3 IRS

Using data from the IRS spectrograph[4] (the Infrared Spectrograph on the *Spitzer Space Telescope*), in Fig. 11 we examined and compared the mid-IR spectrum of HD 44892 (PI: Bouwman, ID 3470) to that of PPDs HD 97048 (PI: Houck, ID 2) and HD 36112 (PI: Bouwman, ID 3470), and debris discs with gas HD 138813 (PI: Carpenter, ID 30091) and HD 131835 (PI: Houck, ID 40651). The spectrum of HD 44892 is quite complex and looks very different to those of both PPD and debris discs, and it shows a distinctive feature at the wavelength of ~ 12 μm, which is not present in the spectra of other objects. The comparison shows that HD 44892 is unique and likely caught at the transition from PPD to debris disc stage.

6 HD 44892 IN THE CONTEXT OF KNOWN GAS-HARBOURING DEBRIS DISCS

In Fig. 12, we compare the dust and CO gas masses we calculated for HD 44892 with Herbig star discs (flux adapted from A. Moór et al. 2017) and all other debris discs with CO gas mass measurements to date (see Table A1 for detailed list), highlighting the discs HD 141569 (J. M. Miley et al. 2018), NO Lup (J. B. Lovell et al. 2021a), Fomalhaut (M. A. MacGregor et al. 2017; L. Matrà et al. 2017b), and η Crv (S. Marino et al. 2017). HD 44892, due to its probable very young age, populates an area where we would expect PPDs to reside, but both its dust and CO gas masses are much lower than expected for PPDs.

Since HD 44892 is younger than almost all of debris discs from Fig. 12, we would expect it to contain more both dust and gas, as less time has passed for collisional evolution and subsequent dispersal of material from the system. While the CO gas mass of our target may be quite high and comparable to the most massive debris discs with gas, the dust mass is lower in comparison. Like HD 141569, HD 44892 is also a pre-MS star. Both these discs seem to represent the missing link between PPDs and the older planetary systems we observe around other stars. They are both at an evolutionary stage following PPDs, suggesting their gas is potentially inherited from this earlier stage, hence is primordial. This does not, however, entirely rule out the possibility of secondary or mixed origin gas.

The accretion rate we derived for HD 44892 (see Section 4.2) is very similar to that measured for HD 141569 (J. R. Fairlamb et al. 2015) and is orders of magnitude higher than expected for CO-rich debris discs (10^{-11}–10^{-13} $M_\odot$ yr^{-1}, Q. Kral et al. 2017; S. P. D. Borthakur et al. 2025). If we assume a secondary origin for the gas, where the gas is H-poor with no significant H_2 reservoir, and adopting the upper limit on the total CO gas mass (based on the ^{13}CO emission) of 10^{-2} $M_\oplus$, the CO in the disc would be depleted within just a few years. It is highly unlikely that a mechanism capable of replenishing such a large amount of secondary gas exists, thus the high accretion rate suggests that at least the inner disc is of primordial origin and dominated by H_2 gas. However, given the accretion variability discussed in Section 4.2, this value may represent a phase of enhanced accretion. A more detailed discussion will be presented in Szewczyk et al. (in prep).

At the young age of HD 44892, apart from HD 141569, only one other comparable ^{12}CO detection in a debris disc exists – that in the disc around NO Lup, a 0.7 $M_\odot$ star with an age estimate of 1–3 Myr. The two other possible ^{12}CO detections presented in J. B. Lovell et al. (2021a), around Sz 108B and Lup 818s, are likely caused by CO cloud (ISM) gas instead. For NO Lup, using continuum and ^{12}CO fluxes from J. B. Lovell et al. (2021a), we derive the CO gas mass, assuming gas temperature of 50 K, of $(5.03 \pm 1.13) \times 10^{-5}$ $M_\oplus$. At the reported dust temperature of 20 K, we estimate the dust mass in the disc to be $(4.00 \pm 1.38) \times 10^{-2}$ $M_\oplus$. These values are comparable to those we derive for HD 44892. HD 44892, similarly to NO Lup, has lost its PPD, but retains some gas and dust. However, given their very different stellar masses and structure, the mechanisms responsible for dispersal are very likely different, i.e. FUV/EUV photoevaporation for the radiative A-type star HD 44892, and X-ray photoevaporation for the convective low-mass star NO Lup (M. Kunitomo et al. 2021).

[4]With reduced spectra obtained from https://cassis.sirtf.com

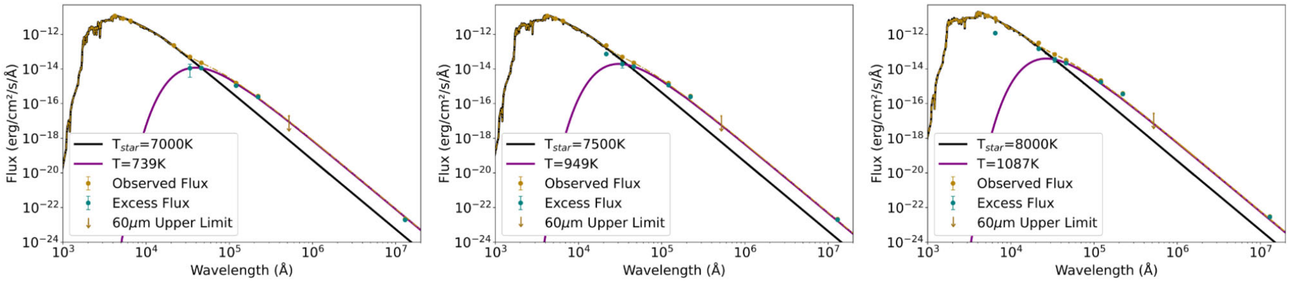

Figure 10. A fit to the SED of HD 44892, for three assumed parent star temperatures: 7000 K (left), 7500 K (middle), and 8000 K (right). These temperatures correspond to the uncertainty range reported by D. P. Iglesias et al. (2023, 7500 ± 500 K). The photometry points used for all plots were *V*, *B*, and *R* photometry, 2MASS ks, *WISE W*1–*W*4 (all from D. P. Iglesias et al. 2023), *IRAS* 60 μm upper limit (VOSA, A. Bayo et al. 2008), and ALMA continuum flux at 1.3 mm as reported here in Section 3.2.1, in order from shortest to longest wavelength. The fitted belt temperatures are shown for each case, using theoretical spectra from VOSA (A. Bayo et al. 2008).

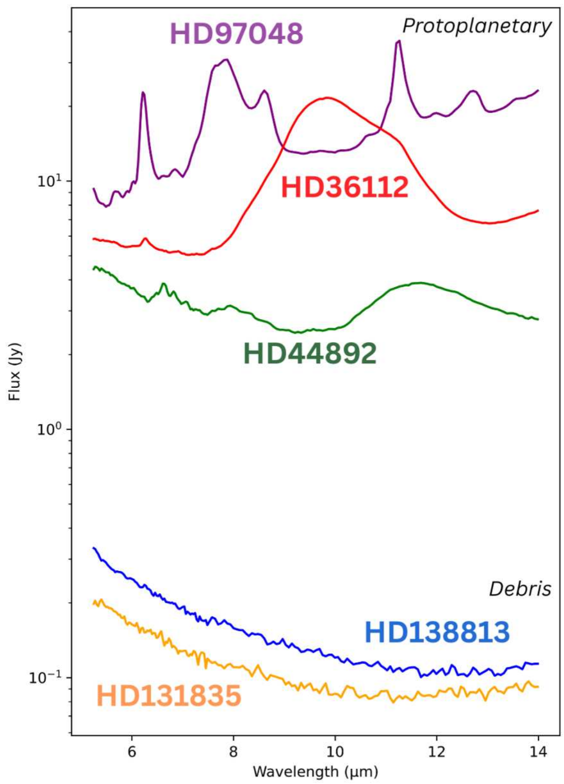

Figure 11. Comparison of mid-IR IRS spectra of HD 44892 with those of PPDs (HD 97048 and HD 36112) and debris discs with gas (HD 138813 and HD 131835), all scaled to 100 pc. HD 44892 looks very different from both PPD and debris discs, being caught in the transition between the two stages.

The probable age of 2.1 Myr makes HD 44892 the youngest known gas-bearing debris disc around an IMS to date. There are several reasons why we trust this age determination the most. First, this object has a relatively high level of fractional IR excess (particularly at 12 μm), putting it in the 'hybrid' category. Such excess is observed to decrease with age, as shown in Fig. 2, and stars older than 100 Myr are expected to have $F_{12\mu m}/F_{\rm star} < 3$. Given HD 44892 has a fractional excess of 7.86 at this wavelength, it is unlikely to be very old, as no debris disc with such a high excess has been found at such an advanced age (see Fig. 2).

Only three debris discs with gas have been found around stars older than 100 Myr: HD 23642 (V∗ V1229 Tau) at 170 Myr (J. Péricaud et al. 2017; J. Southworth et al. 2023), Fomalhaut (HD 216956) at 440 Myr (L. Matrà et al. 2017b), and the 1–2 Gyr η Crv (S. Marino et al. 2017). The older age possibility of HD 44892, at 800 Myr, would make it comparable to the latter two of these objects. For Fomalhaut, using data from L. Matrà et al. (2017b) and M. A. MacGregor et al. (2017), we derive a 50 K dust mass of $(1.49 \pm 0.38) \times 10^{-2}\,M_\oplus$ and a CO gas mass of $(1.89 \pm 0.55) \times 10^{-7} M_\oplus$. For η Crv, we derive a dust mass at 50 K of $(1.07 \pm 0.87) \times 10^{-2}\,M_\oplus$ and a CO gas mass of $(5.92 \pm 0.78) \times 10^{-7}\,M_\oplus$ (with flux data from S. Marino et al. 2017). Both systems contain at least three orders of magnitude less CO gas mass than HD 44892 (see Fig. 12). This further shows that if HD 44892 was 800 Myr, it would be an outlier, containing significantly high amounts of CO gas.

It is worth noting that discs exist around post-asymptotic giant branch (AGB) binary star systems, with dust masses even up to 1 M_J (J. Kluska et al. 2022). These, however, are created from the mass loss of primary object during the last stages of its evolution. HD 44892, at the age of 2.1 Myr, is approaching the zero-age main sequence or, at the alternative age of 800 Myr, is crossing the HR gap after leaving the MS. Both its stellar temperature and luminosity are inconsistent with the star being on the AGB. Moreover, there is no evidence to suggest that HD 44892 is a binary system, hence this scenario is inapplicable here.

7 SUMMARY AND FUTURE PROSPECTS

Using ALMA, we have detected CO emission in a debris disc around a young, pre-MS IMS HD 44892 with a fractional IR excess of $7.86^{+0.11}_{-2.27}$ at 12 μm (D. P. Iglesias et al. 2023), which falls within a range ($3 < F_{12\mu m}/F_{\rm star} < 25$) where only one such object, HD 141569, has been previously identified with a measured CO gas mass. This provides a rare glimpse into the very stage of transition from PPD to debris discs. HD 44892 is hence also one of the youngest known hybrid discs, along with the lower mass ($0.7\,M_\odot$) star NO Lup, with an age 1–3 Myr (J. B. Lovell et al. 2021a). For gas temperature in the range 20–50 K, the CO detection yields an estimate of CO gas mass of around $10^{-4}\,M_\oplus$. On the other hand, the non-detections of ^{13}CO and C^{18}O lines provide upper limits on gas mass of around $10^{-2}\,M_\oplus$. Since we do not know whether the ^{12}CO emission we detected is optically thin or thick, the CO gas mass we derived from ^{12}CO emission should be treated as a lower limit, and may be up to $\sim 10^{-2}\,M_\oplus$, which is the upper limit derived from ^{13}CO non-detection.

Given the possibility of the primordial origin of gas, we also report the total gas mass values, calculated assuming an ISM ratio of $^{12}CO/H_2 = 10^{-4}$ in the disc. This results in total H_2 gas mass

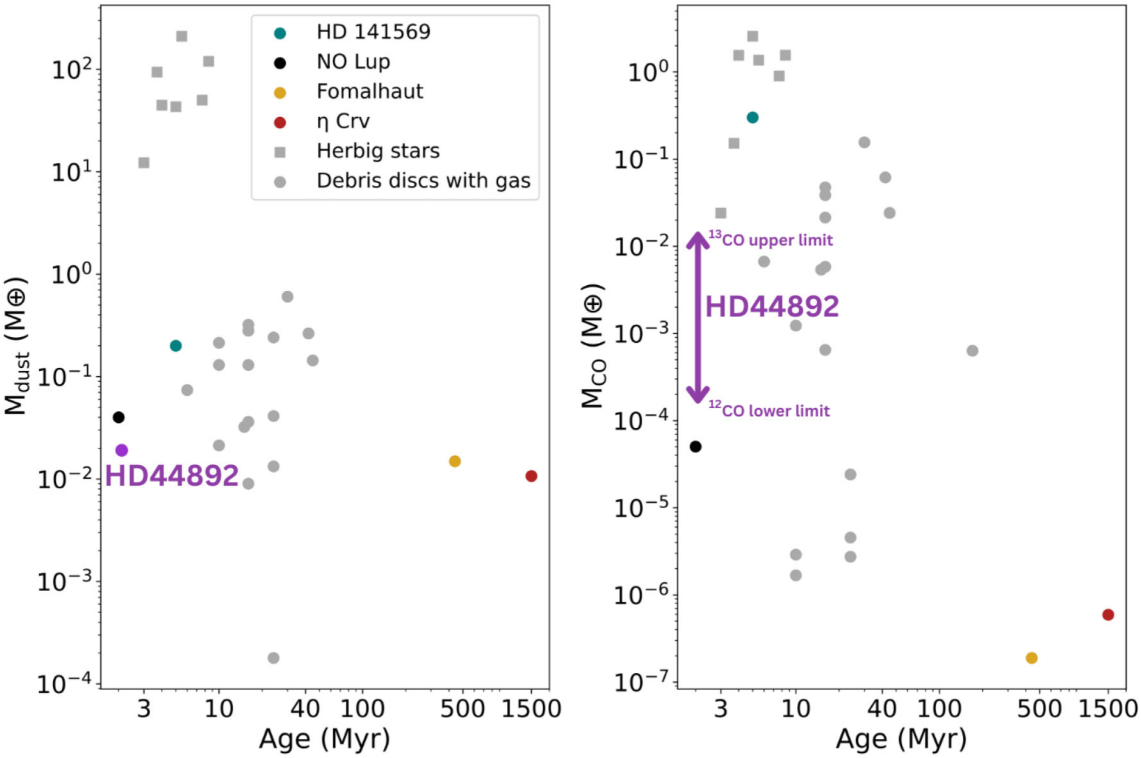

Figure 12. Comparison of the dust and CO masses of HD 44892 with other known debris discs hosting CO gas (circular points) and fainter Herbig star discs (square points, adapted from A. Moór et al. (2017), calculated for $T = 25$ K). For reference we marked: the hybrid disc HD 141569, with a dust mass of $0.20 \pm 0.07\,M_\oplus$ and a CO gas mass of $(3.01 \pm 0.48) \times 10^{-1}\,M_\odot$ (J. M. Miley et al. 2018); NO Lup, assumed to be 2 Myr old for this plot, which has a CO gas mass of $(5.03 \pm 1.12 \times 10^{-5}\,M_\oplus$ and a dust mass of $(4.00 \pm 1.38) \times 10^{-2}\,M_\oplus$ (J. B. Lovell et al. 2021a); Fomalhaut, at 440 Myr, which has a CO gas mass of $(1.89 \pm 0.55) \times 10^{-7}\,M_\oplus$ and a dust mass of $(1.49 \pm 0.38) \times 10^{-2} M_\oplus$ (M. A. MacGregor et al. 2017; L. Matrà et al. 2017b); lastly, the 1–2 Gyr-old system η Crv, assumed to be 1.5 Gyr for this plot, which has a CO gas mass of $(5.92 \pm 0.78) \times 10^{-7} M_\oplus$ and a dust mass of $(1.07 \pm 0.87) \times 10^{-2} M_\oplus$ (S. Marino et al. 2017). All CO gas masses of debris discs with gas have been derived using a gas temperature of 50 K, while for dust masses we used corresponding dust temperatures for each object. Remaining CO and dust fluxes used were adapted from from Á. Kóspál et al. (2013); A. Moór et al. (2013, 2017, 2019); W. R. F. Dent et al. (2014); J. Lieman-Sifry et al. (2016); S. Marino et al. (2016); K. Y. L. Su et al. (2017); L. Matrà et al. (2017a, 2019); J. M. Miley et al. (2018); A. Bayo et al. (2019); and I. Rebollido et al. (2022); see Table A1 for details.

of $0.06 \pm 0.02\,M_\oplus$ for 20 K gas and $0.12 \pm 0.01\,M_\oplus$ for 50 K gas, yielding a gas-to-dust mass ratio of ~3 at 20 K or ~6 at 50 K. The H_2 masses presented are based on ^{12}CO emission, which may be optically thick, and hence represent lower limits to the total disc gas mass. However, if this gas is of secondary rather than primordial origin, this ratio does not apply, since secondary gas is hydrogen-depleted (G. V. Smirnov-Pinchukov et al. 2022). In such a case, the gas is most likely CO dominated, making the CO gas mass a better representative of the total disc gas mass.

Presence of circumstellar gas is further confirmed in our UVES observations of gas absorption, for which we were able to rule out interstellar origin. From the UVES data, we also derived an accretion rate for HD 44892 of $\log \dot{M}_{\rm acc} = -7.64^{+0.11}_{-0.07}$ and $-7.69^{+0.11}_{-0.07}\,M_\odot\,{\rm yr}^{-1}$ for the two observed epochs. This value is comparable to that of HD 141569 exceeding the level expected for CO-rich debris discs and is similar to values found in PPDs. If the gas was secondary, then based on the $\sim 10^{-2}\,M_\oplus$ CO gas mass upper limit, from our ^{13}CO non-detection, it would be depleted on very short time–scales, and replenishment at the required rate seems unlikely. This strongly suggests that at least the inner disc retains primordial, H_2-rich gas.

We also detect 1.3 mm continuum emission in HD 44892 in our ALMA observations. We report the dust mass of HD 44892, assuming a dust temperature of 115 K, of $0.019 \pm 0.009\,M_\oplus$. Millimetre dust in this young disc is likely to originate from collisional evolution, given the collisional dust lifetime we estimate at $\sim 10^{-2}$ Myr. With the detected 1.3 mm flux and known shorter wavelength photometric measurements of HD 44892, along with the stellar spectrum models, we attempt to characterize the SED in the context of single-temperature ring models. This approach suggests that almost all of the excess emission comes from hot material, over 700 K, thus close to the star. Indeed, most of the millimetre flux in HD 44892 is unresolved and may originate from a point source.

If this is correct, then the marginally resolved dust and gas extending at ~40–45 au are very cold and vertically thin enough not to intercept stellar light – the only scenario to explain the lack of significant IR emission from these spatial scales. Such flattened disc structures (and low-excess SEDs) may arise at late stages of PPD evolution due to gas loss but also when all the very small, submicrometre dust has been removed (O. Panić & M. Min 2017). Important to note is that removal of such dust creates conditions for gas survival beyond PPD phase suggested by R. Nakatani et al. (2021). Assuming HD 44892 is an example of this scenario, future studies could involve scattered-light observations using telescopes such as the VLT/SPHERE (Spectro-Polarimetric High-contrast Exoplanet REsearch), to verify if such small grains are indeed absent from its debris disc by, for example, if scattered light is absent, or has a colour indicative of scattering by larger grains (G. D. Mulders et al. 2013).

The dust mass in the disc of HD 44892 is within an order of magnitude less than that of the hybrid disc HD 141569. The CO gas mass may be comparable to that of known gas-rich debris discs, depending on the optical thickness of ^{12}CO emission. Given the very young age of HD 44892, primordial origin gas is likely (R. Nakatani et al. 2021; G. V. Smirnov-Pinchukov et al. 2022). Hence, it is possible that we have caught this disc just at the end of its primordial gas contents, which may explain the relatively low CO mass. This suggests HD 44892 is the next evolutionary stage following HD 141569, helping us understand the evolution of planetary systems better. None the less, the young age of this object alone does not allow to make definitive conclusions about the origin of gas in this disc.

It is important to note that from the CO gas mass alone, of $(1.62 \pm 0.17) \times 10^{-4}\,M_{\oplus}$, it is impossible to fully rule out the secondary origin scenario. According to G. Cataldi et al. (2023), only CO-rich debris discs, which they classify as having $M_{CO} \gtrsim 10^{-3}\,M_{\oplus}$, cannot be solely explained by the current secondary models (like the one in Q. Kral et al. 2017). A solution may be either an improvement of secondary models of gas production or presence of primordial gas. On the other hand, they state that it is the debris discs with low CO gas masses, $\lesssim 10^{-5}\,M_{\oplus}$ that are easily explainable by secondary means alone. Since the CO gas mass of HD 44892 is between the two, secondary or mixed origin is still possible. It is worth noting, however, that while models introduced in Q. Kral et al. (2019) can explain the high CO gas masses in CO-rich debris discs, by introducing neutral carbon shielding and self-shielding of CO, more recent work of S. Marino et al. (2022) discusses the limitations of this scenario. In particular, they show that vertical mixing of gas in the debris disc reduces the effectiveness of shielding, limiting the accumulation of CO. Hence, for the most CO-rich systems secondary models alone are not yet able to explain this gas presence, and primordial origin remains the best available explanation (S. Marino et al. 2022; G. Cataldi et al. 2023). G. Cataldi et al. (2023) propose that observations of C I in debris discs where CO was found are needed to improve current models of gas, which might help answer questions regarding its origin. Since HD 44892 has a CO gas mass comparable to some of the debris discs with detected C I in their sample, it is possible that HD 44892 may also have detectable C I emission in higher sensitivity observations.

If the alternative age of 800 Myr is considered, HD 44892 would be an outlier in terms of its dust mass (temperature-dependent), 12 μm excess, and CO gas mass, strongly suggesting that this is the case of a young pre-MS star. The two proposed age scenarios, of 2.1 and 800 Myr, correspond to different stellar mass estimates of 2.87 and $2.29\,M_{\odot}$, respectively. Future, higher spatial and spectral resolution studies of CO emission with ALMA, could remove any remaining uncertainties, allowing for a dynamical mass estimation of the star.

ACKNOWLEDGEMENTS

KS acknowledges funding from the Bell Burnell Graduate Scholarship Fund (BB0023). OP and DPI acknowledge support from the Science and Technology Facilities Council via grant no. ST/X001016/1. TDP is supported by a UKRI Stephen Hawking Fellowship and a Warwick Prize Fellowship, the latter made possible by a generous philanthropic donation. JM acknowledges support from FONDECYT de Postdoctorado 2024 no. 3240612 and ANID – Millennium Science Initiative Program – Center Code NCN2024_001.

We thank Lionell Siess, Sebastian Marino, Rens Waters, and Till Käufer for fruitful discussions.

We thank the anonymous referee for their insightful comments and suggestions, which provided valuable perspectives on the nature of this system.

This paper makes use of the following ALMA data: ADS/JAO.ALMA no. 2022.1.01686.S ALMA is a partnership of ESO (representing its member states), NSF (USA), and NINS (Japan). It includes NRC (Canada), MOST and ASIAA (Taiwan), and KASI (Republic of Korea), in cooperation with the Republic of Chile. The Joint ALMA Observatory is operated by ESO, AUI/NRAO, and NAOJ.

Based on observations collected at the European Southern Observatory under ESO programmes 112.262.P.001, 094.A-9029(D), 082.D-0499(A), and 085.D-0395(A).

This work has made use of data from the European Space Agency (ESA) mission *Gaia* (https://www.cosmos.esa.int/gaia), processed by the *Gaia* Data Processing and Analysis Consortium (DPAC, https://www.cosmos.esa.int/web/gaia/dpac/consortium). Funding for the DPAC has been provided by national institutions, in particular the institutions participating in the *Gaia* Multilateral Agreement.

This publication makes use of VOSA, developed under the Spanish Virtual Observatory (https://svo.cab.inta-csic.es) project funded by MCIN/AEI/10.13039/501100011033/ through grant PID2020-112949GB-I00. VOSA has been partially updated by using funding from the European Union's Horizon 2020 Research and Innovation Programme, under grant agreement no. 776403 (EXOPLANETS-A).

This research has made use of the SIMBAD database, operated at CDS, Strasbourg, France.

This work is based [in part] on observations made with the *Spitzer Space Telescope*, which was operated by the Jet Propulsion Laboratory, California Institute of Technology under a contract with NASA.

DATA AVAILABILITY

All data underlying this article are available at the ALMA, ESO, and *Gaia* archives. ALMA data are found under project 2022.1.01686.S at https://almascience.eso.org/aq/. ESO data are found under projects 112.262.P.001, 094.A-9029(D), 082.D-0499(A), and 085.D-0395(A) at http://archive.eso.org/cms.html. *Gaia* archive can be browsed at https://gea.esac.esa.int/archive. *Spitzer* IRS spectra can be found at https://cassis.sirtf.com.

REFERENCES

Abt H. A., Moyd K. I., 1973, ApJ, 182, 809
Allende Prieto C., Lambert D. L., 1999, A&A, 352, 555
Ballester P., Modigliani A., Boitquin O., Cristiani S., Hanuschik R., Kaufer A., Wolf S., 2000, The Messenger, 101, 31
Bayo A. et al., 2019, MNRAS, 486, 5552
Bayo A., Rodrigo C., Barrado Y Navascués D., Solano E., Gutiérrez R., Morales-Calderón M., Allard F., 2008, A&A, 492, 277
Beckwith S. V. W., Sargent A. I., Chini R. S., Guesten R., 1990, AJ, 99, 924
Bochanski J. J., Faherty J. K., Gagné J., Nelson O., Coker K., Smithka I., Desir D., Vasquez C., 2018, AJ, 155, 149
Borthakur S. P. D., Kama M., Fossati L., Kral Q., Folsom C. P., Teske J., Aret A., 2025, A&A, 697, A59
Cataldi G. et al., 2023, ApJ, 951, 111
Chen C. H., Jura M., 2003, ApJ, 582, 443
Comrie A. et al., 2021, CARTA: The Cube Analysis and Rendering Tool for Astronomy. Zenodo
Dekker H., D'Odorico S., Kaufer A., Delabre B., Kotzlowski H., 2000, in Iye M., Moorwood A. F. eds, Proc. SPIE Conf. Ser., Vol. 4008, Optical and

IR Telescope Instrumentation and Detectors. SPIE, Bellingham, WA, p. 534
Dent W. R. F. et al., 2014, Science, 343, 1490
Di Folco E., Péricaud J., Dutrey A., Augereau J. C., Chapillon E., Guilloteau S., Piétu V., Boccaletti A., 2020, A&A, 635, A94
Esposito T. M. et al., 2020, AJ, 160, 24
Fairlamb J. R., Oudmaijer R. D., Mendigutía I., Ilee J. D., van den Ancker M. E., 2015, MNRAS, 453, 976
Fairlamb J. R., Oudmaijer R. D., Mendigutia I., Ilee J. D., van den Ancker M. E., 2017, MNRAS, 464, 4721
Freudling W., Romaniello M., Bramich D. M., Ballester P., Forchi V., García-Dabló C. E., Moehler S., Neeser M. J., 2013, A&A, 559, A96
Gagné J. et al., 2018, ApJ, 856, 23
Gaia Collaboration, 2016, A&A, 595, A1
Gaia Collaboration, 2023, A&A, 674, A1
Gontcharov G. A., 2006, Astron. Lett., 32, 759
Hales A. S. et al., 2022, ApJ, 940, 161
Hughes A. M., Duchêne G., Matthews B. C., 2018, ARA&A, 56, 541
Iglesias D. et al., 2018, MNRAS, 480, 488
Iglesias D. P. et al., 2019, MNRAS, 490, 5218
Iglesias D. P. et al., 2023, MNRAS, 519, 3958
Iglesias D., 2020, Searching for Gas in Debris Disks, Zenodo
Inutsuka S.-i., Aikawa Y., Muto T., Tomida K., Tamura M. eds, 2023, Protostars and Planets VII. Astron. Soc. Pac., San Francisco, CA
Ishihara D., Takeuchi N., Kobayashi H., Nagayama T., Kaneda H., Inutsuka S.-i., Fujiwara H., Onaka T., 2017, A&A, 601, A72
Kaufer A., Stahl O., Tubbesing S., Nørregaard P., Avila G., Francois P., Pasquini L., Pizzella A., 1999, The Messenger, 95, 8
Kausch W. et al., 2015, A&A, 576, A78
Kiefer F., Lecavelier des Etangs A., Augereau J. C., Vidal-Madjar A., Lagrange A. M., Beust H., 2014b, A&A, 561, L10
Kiefer F., Lecavelier des Etangs A., Boissier J., Vidal-Madjar A., Beust H., Lagrange A. M., Hébrard G., Ferlet R., 2014a, Nature, 514, 462
Kluska J., Van Winckel H., Coppée Q., Oomen G. M., Dsilva K., Kamath D., Bujarrabal V., Min M., 2022, A&A, 658, A36
Kóspál Á. et al., 2013, ApJ, 776, 77
Koubsky P., Horn J., Harmanec P., Hubert A. M., Hubert H., Floquet M., 1993, A&A, 277, 521
Kral Q., Marino S., Wyatt M. C., Kama M., Matrà L., 2019, MNRAS, 489, 3670
Kral Q., Matrà L., Wyatt M. C., Kennedy G. M., 2017, MNRAS, 469, 521
Kunitomo M., Ida S., Takeuchi T., Panić O., Miley J. M., Suzuki T. K., 2021, ApJ, 909, 109
Lagrange-Henri A. M., Ferlet R., Vidal-Madjar A., Beust H., Gry C., Lallement R., 1990, A&AS, 85, 1089
Lebreton J. et al., 2013, A&A, 555, A146
Lieman-Sifry J., Hughes A. M., Carpenter J. M., Gorti U., Hales A., Flaherty K. M., 2016, ApJ, 828, 25
Lovell J. B. et al., 2021a, MNRAS, 500, 4878
Lovell J. B. et al., 2021b, MNRAS, 502, L66
MacGregor M. A. et al., 2017, ApJ, 842, 8
Malamut C., Redfield S., Linsky J. L., Wood B. E., Ayres T. R., 2014, ApJ, 787, 75
Marino S. et al., 2016, MNRAS, 460, 2933
Marino S. et al., 2017, MNRAS, 465, 2595
Marino S., Cataldi G., Jankovic M. R., Matrà L., Wyatt M. C., 2022, MNRAS, 515, 507
Matrà L. et al., 2017a, MNRAS, 464, 1415
Matrà L. et al., 2017b, ApJ, 842, 9
Matrà L., Marino S., Kennedy G. M., Wyatt M. C., Öberg K. I., Wilner D. J., 2018, ApJ, 859, 72
Matrà L., Öberg K. I., Wilner D. J., Olofsson J., Bayo A., 2019, AJ, 157, 117
Matrà L., Panić O., Wyatt M. C., Dent W. R. F., 2015, MNRAS, 447, 3936
Mayor M. et al., 2003, The Messenger, 114, 20
McMullin J. P., Waters B., Schiebel D., Young W., Golap K., 2007, in Shaw R. A., Hill F., Bell D. J. eds, Astronomical Data Analysis Software and Systems XVI, Vol. 376. ASP Conf. Ser., San Francisco, CA, p. 127
Miley J. M., Panić O., Haworth T. J., Pascucci I., Wyatt M., Clarke C., Richards A. M. S., Ratzka T., 2019, MNRAS, 485, 739
Miley J. M., Panić O., Wyatt M., Kennedy G. M., 2018, A&A, 615, L10
Montgomery S. L., Welsh B. Y., 2012, PASP, 124, 1042
Moór A. et al., 2013, ApJ, 777, L25
Moór A. et al., 2017, ApJ, 849, 123
Moór A. et al., 2019, ApJ, 884, 108
Mulders G. D., Min M., Dominik C., Debes J. H., Schneider G., 2013, A&A, 549, A112
Nakatani R., Kobayashi H., Kuiper R., Nomura H., Aikawa Y., 2021, ApJ, 915, 90
Panić O. et al., 2013, MNRAS, 435, 1037
Panić O., Min M., 2017, MNRAS, 467, 1175
Pearce T. D. et al., 2022, A&A, 659, A135
Pearce T. D., Beust H., Faramaz V., Booth M., Krivov A. V., Löhne T., Poblete P. P., 2021, MNRAS, 503, 4767
Pearce T. D., Krivov A. V., Booth M., 2020, MNRAS, 498, 2798
Péricaud J., Di Folco E., Dutrey A., Guilloteau S., Piétu V., 2017, A&A, 600, A62
Rebollido I. et al., 2018, A&A, 614, A3
Rebollido I. et al., 2020, A&A, 639, A11
Rebollido I. et al., 2022, MNRAS, 509, 693
Redfield S., 2007, ApJ, 656, L97
Rhee J. H., Song I., Zuckerman B., McElwain M., 2007, ApJ, 660, 1556
Riviere-Marichalar P. et al., 2014, A&A, 565, A68
Roberge A., Welsh B. Y., Kamp I., Weinberger A. J., Grady C. A., 2014, ApJ, 796, L11
Sandell G., Weintraub D. A., Hamidouche M., 2011, ApJ, 727, 26
Schneiderman T. et al., 2021, Nature, 598, 425
Sezestre É., Augereau J. C., Thébault P., 2019, A&A, 626, A2
Sheret I., Dent W. R. F., Wyatt M. C., 2004, MNRAS, 348, 1282
Smette A. et al., 2015, A&A, 576, A77
Smirnov-Pinchukov G. V., Moór A., Semenov D. A., Ábrahám P., Henning T., Kóspál Á., Hughes A. M., di Folco E., 2022, MNRAS, 510, 1148
Southworth J., Murphy S. J., Pavlovski K., 2023, MNRAS, 520, L53
Squicciarini V. et al., 2025, A&A, 693, A54
Stapper L. M., Hogerheijde M. R., van Dishoeck E. F., Mentel R., 2022, A&A, 658, A112
Su K. Y. L. et al., 2017, AJ, 154, 225
Welsh B. Y., Craig N., Crawford I. A., Price R. J., 1998, A&A, 338, 674
Welsh B. Y., Montgomery S. L., 2015, Adv. Astron., 2015, 980323
Welsh B. Y., Montgomery S. L., 2018, MNRAS, 474, 1515
Welsh B. Y., Montgomery S., 2013, PASP, 125, 759
Wenger M. et al., 2000, A&AS, 143, 9
Wichittanakom C., Oudmaijer R. D., Fairlamb J. R., Mendigutía I., Vioque M., Ababakr K. M., 2020, MNRAS, 493, 234
Wilson T. L., Rood R., 1994, ARA&A, 32, 191
Wyatt M. C., Dent W. R. F., 2002, MNRAS, 334, 589
Wyatt M. C., Panić O., Kennedy G. M., Matrà L., 2015, Ap&SS, 357, 103
Zorec J., Royer F., 2012, A&A, 537, A120

APPENDIX A: DEBRIS DISCS WITH GAS FOUND THROUGH EMISSION

Table A1. [e] denotes references for gas emission detections, while [a] refers to gas absorption discoveries in discs that also exhibit gas emission. Dust and CO gas masses were uniformly calculated across the sample. For CO gas mass, we assumed a uniform gas temperature $T = 50$ K. Where available, the CO gas mass estimates are based on observations of rarer isotopologues. For dust mass, we used dust temperatures derived for corresponding targets, with dust opacity assumed as $\kappa = 0.1 \times 2.3 \times (\frac{\nu}{230\times10^9})^{0.7}$ [cm^2 g^{-1}] (S. V. W. Beckwith et al. 1990), where ν is the frequency of observations [Hz].

Name	Age (Myr)	Stellar mass ($M_\odot$)	Spectral type	Distance (pc)	Dust mass ($M_\oplus$)	CO gas mass ($M_\oplus$)	Reference
V∗ NO Lup	1–3	0.7	K7	132.90	4.00×10^{-2}	5.03×10^{-5}	J. B. Lovell et al. (2021a)[e]
HD 44892	2.1	2.87	A9/F0IV	191.00	1.91×10^{-2}	1.62×10^{-4}	This study
HD 141569	5	2.04[1]	A2VekB9mB9(_lB)	111.61	2.00×10^{-1}	3.01×10^{-1}	J. M. Miley et al. (2018)[e]; C. Malamut et al. (2014)[a]
HD 36546	3–10	1.87[2]	B8	100.18	7.40×10^{-2}	6.69×10^{-3}	I. Rebollido et al. (2022)[e]; I. Rebollido et al. (2020)[a]
V∗ CE Ant	10	0.31[1]	M2Ve	34.10	2.13×10^{-2}	1.68×10^{-6}	L. Matrà et al. (2019)[e]
HD 138813	10[3]	2.15[3]	A0V	136.60	1.30×10^{-1}	1.23×10^{-3}	J. Lieman-Sifry et al. (2016)[e]
HD 146897	10[3]	1.32[3]	F2/3V	132.19	2.14×10^{-1}	2.90×10^{-6}	J. Lieman-Sifry et al. (2016)[e]
HD 172555	24[3]	1.71[3]	A7V	28.79	1.79×10^{-4}	4.56×10^{-6}	T. Schneiderman et al. (2021)[e]; F. Kiefer et al. (2014b)[a]
HD 110058	15[3]	1.53[3]	A0V	130.08	3.23×10^{-2}	5.40×10^{-3}	A. S. Hales et al. (2022)[e]; D. Iglesias et al. (2018)[a]
HD 121191	16[3]	1.63[3]	A5IV/V	132.29	9.02×10^{-3}	5.83×10^{-3}	A. Moór et al. (2017)[e]
HD 121617	16[3]	1.90[3]	A1V	117.89	1.30×10^{-1}	3.86×10^{-2}	A. Moór et al. (2017)[e]
HD 131488	16[4]	1.8[6]	A1V	152.24	3.21×10^{-1}	4.75×10^{-2}	A. Moór et al. (2017)[e]
HD 131835	16[3]	1.81[3]	A2IV	129.74	2.81×10^{-1}	2.14×10^{-2}	J. Lieman-Sifry et al. (2016)[e]
HD 156623	16[3]	1.91[3]	A0V	108.33	3.62×10^{-2}	6.48×10^{-4}	J. Lieman-Sifry et al. (2016)[e]; I. Rebollido et al. (2018)[a]
HD 181327	24	1.36	F6V	47.78	2.41×10^{-1}	2.70×10^{-6}	S. Marino et al. (2016)[e]
∗ bet Pic	24[7]	1.73[1]	A6V	19.63	4.13×10^{-2}	2.41×10^{-5}	W. R. F. Dent et al. (2014)[e]; F. Kiefer et al. (2014a)[a]
∗ eta Tel	24[3]	2.21[3]	A0V	48.54	1.33×10^{-2}	–	P. Riviere-Marichalar et al. (2014)[e]; I. Rebollido et al. (2018)[a]
HD 32297	<30	1.69[1]	A0V	129.73	6.04×10^{-1}	1.56×10^{-1}	A. Moór et al. (2019)[e]; S. Redfield (2007)[a]
∗ 49 Cet	45[3]	1.98[3]	A1V	57.23	1.44×10^{-1}	2.42×10^{-2}	A. Moór et al. (2019)[e]; A. Roberge et al. (2014)[a]
HD 21997	42[3]	1.83[3]	A3IV/V	69.69	2.64×10^{-1}	6.17×10^{-2}	Á. Kóspál et al. (2013)[e]
V∗ V1229 Tau	170[5]	–	A0VpSi + Am	138.31	–	6.33×10^{-4}	J. Péricaud et al. (2017)[e]
HD 216956	440	1.9[6]	A4V	7.70	1.49×10^{-2}	1.89×10^{-7}	L. Matrà et al. (2017b)[e]
∗ eta Crv	1000–2000	1.39[3]	F2V	18.24	1.07×10^{-2}	5.92×10^{-7}	S. Marino et al. (2017)[e]

Notes. Stellar ages and masses are adopted from the listed references unless indicated otherwise. Spectral types and distances were obtained from SIMBAD (M. Wenger et al. 2000). We do not report CO gas mass for ∗ eta Tel, which has [C II] emission. For V∗ V1229 Tau no continuum emission was detected, hence we do not report the dust mass in this disc. We did not find a reliable stellar mass estimate for V ∗ V1229 Tau. Gas absorption detections and their references were adopted from D. Iglesias (2020, table 1.1). Additional references for stellar age and mass: [1] T. M. Esposito et al. (2020), [2] C. Allende Prieto & D. L. Lambert (1999), [3] T. D. Pearce et al. (2022), [4] A. Moór et al. (2017), [5] J. Southworth, S. J. Murphy & K. Pavlovski (2023), [6] L. Matrà et al. (2018), and [7] V. Squicciarini et al. (2025).

This paper has been typeset from a TEX/LATEX file prepared by the author.